

Review

## Organic / IV, III-V Semiconductor Hybrid Solar Cells

Pang-Leen Ong<sup>1</sup> and Igor A. Levitsky<sup>1,2,\*</sup>

<sup>1</sup> Emitech, Inc., Fall River, Massachusetts, 02720, USA; E-Mail: pangleen@emitechinc.com

<sup>2</sup> Department of Chemistry, University of Rhode Island, Kingston, Rhode Island, 02881, USA

\* Author to whom correspondence should be addressed; E-Mail: ilevitsky@emitechinc.com;  
Tel.: +01-508-324-0758; Fax: +01-508-324-1139.

Received: 30 December 2009; in revised form: 5 February 2010 / Accepted: 5 February 2010 /

Published: 5 March 2010

---

**Abstract:** We present a review of the emerging class of hybrid solar cells based on organic-semiconductor (Group IV, III-V), nanocomposites, which states separately from dye synthesized, polymer-metal oxides and organic-inorganic (Group II-VI) nanocomposite photovoltaics. The structure of such hybrid cell comprises of an organic active material (*p*-type) deposited by coating, printing or spraying technique on the surface of bulk or nanostructured semiconductor (*n*-type) forming a heterojunction between the two materials. Organic components include various photosensitive monomers (e.g., phthalocyanines or porphyrines), conjugated polymers, and carbon nanotubes. Mechanisms of the charge separation at the interface and their transport are discussed. Also, perspectives on the future development of such hybrid cells and comparative analysis with other classes of photovoltaics of third generation are presented.

**Keywords:** hybrid solar cells; photovoltaic effect; solar energy; organic-inorganic solar cells; Group IV, III-V semiconductors; carbon nanotubes

---

### 1. Introduction

To date, organic and organic-inorganic photovoltaics (PVs) (third generation solar cells) continue to attract great attention from the PV community, due to their promising features such as low fabrication cost, flexibility and light weight. Third generation solar cells follows the second generation (thin film inorganics such as amorphous silicon (a-Si), cadmium telluride (CdTe), and copper indium gallium selenide (CIGS)) and first generation (semiconducting, crystalline) PVs. The class of organic PVs

includes devices with flat and bulk heterojunction between the various types of conjugated polymers, small molecules, fullerene derivatives, and carbon nanotubes [1-3]. Despite substantial progress in solar cell architecture, design and rational choice of the donor-acceptor materials over the past two decades, organic PVs are still unable to overcome the 6–7% barrier of conversion efficiency [4,5]. In terms of the low conversion efficiency, there are currently at least four major fundamental aspects making organic PVs vulnerable for commercial applications as compared with conventional semiconducting solar cells: (i) low carrier mobility, (ii) lack of absorption in the red/NIR part of spectrum, (iii) poor environmental stability, and (iv) excitonic character of photocarrier generation. If the first three above-mentioned statements are obvious, the fourth requires some explanation.

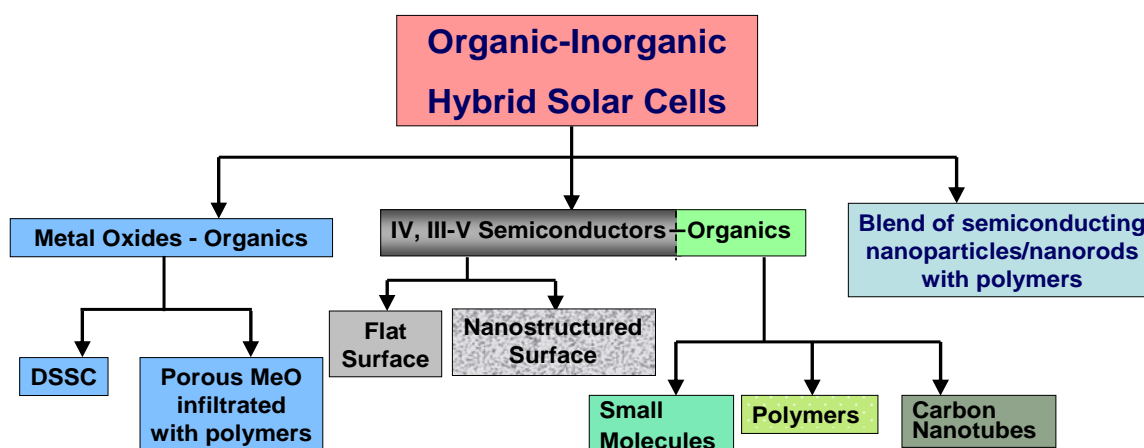
The source of photocarriers in organics is small radius excitons generated as a result of photon absorption. Excitons in organics have a binding energy in the range 200–400 meV [6,7], which is considerably higher than the binding exciton energy for semiconductor materials ~2–40 meV [8]. Thermal energy at room temperature is not sufficient (~25 meV) for exciton dissociation to hole and electron in the bulk medium. Therefore, exciton dissociation should occur at the interface between the donor and acceptor materials with proper HOMO and LUMO energy levels. The mechanism of exciton dissociation is not completely understood, however the major factor governing the charge separation at the interface is the charge transfer process between the donor and acceptor components. After charge separation, holes and electrons move to the opposite electrodes owing to drift (induced by the electric field at the interface) and diffusion (gradient of the charge concentration from the interface to the surface). In the case of a flat heterojunction, the diffusion length of the singlet excitons (several tens nanometers) should be comparable with the thickness of at least of one active layer (donor or acceptor) to minimize energy loss, otherwise not all excitons are able to reach the interface. However, at such small thickness, the absorbed energy is very low since the penetration length of incident light for organics is typically more than 100 nm. The possible solution could be formation of bulk heterojunctions (blend of donor and acceptor materials) with separation scale factor comparable with the excitonic diffusion lengths and relatively thick films to absorb more light energy. Nevertheless, an increase of the film thickness should result in a longer photocarrier pathway to the external electrodes, which reduces the conversion efficiency owing to carriers trapping and lower carrier mobility.

An alternative to pure organic PVs is the class of organic-inorganic hybrid solar cells [9-12], where heterojunction is formed between inorganic semiconductors and organic compounds (small molecules, oligomers, polymers, carbon nanotubes). An advantage of hybrid PVs over organics PVs lies in the high carrier mobility of the semiconductor and the light absorption at longer wavelengths than for organic compounds. On the other hand, the existence of the organic component allows hybrid solar cells to be superior over conventional semiconducting PVs in terms of cost efficiency, scalable wet processing, the variety of organic materials (mismatch between inorganic components can be minimized or prevented), light weight, and flexibility. Moreover, the recent progress in advanced semiconducting nanostructures in combination with organic nanomaterials [e.g., fullerenes and carbon nanotubes (CNTs)] opens new opportunities to overcome the 10% barrier of conversion efficiency for hybrid solar cells in the near future. Note, that band engineering can be a useful instrument in the design of the hybrid solar cell architecture, however it is not as straightforward as for semiconducting PVs. For example, the chemical functionalizing of the organic component (introduction of reducing or oxidizing groups in the chemical structure) is capable of significantly affecting the band gap energy

and position of the Fermi level for conducting polymers and small molecules. Even physical doping (e.g., by simple exposure of polymer film upon iodine vapors) can strongly increase the polymer conductivity and reduce its transparency, thus altering the polymer optoelectronic properties. Thus, the PV performance of hybrid solar cell can be readily optimized by tuning the band structure of organic component (work function, band gap, Fermi level) for the best matching with the corresponding band structure of the inorganic counterpart.

Figure 1 systemizes the types of hybrid PVs depending on the nature of organic and inorganic component and the morphology of the devices. This review is focused on hybrid solar cells based on Group IV (Si) and Group III-V (mostly GaAs) semiconductors forming the heterojunction with various organic components. However, for generality purposes, we will briefly describe other types of hybrid PVs.

**Figure 1.** Classification of hybrid solar cells.



Dye-sensitized solar cells (DSSCs) [9,11] is probably the most well studied hybrid solar cells. DSSC is composed of nanoporous metal oxide (usually  $\text{TiO}_2$ ) infiltrated with sensitized dye molecules (ruthenium based “N<sub>3</sub>” dye) and liquid electrolyte. Photon absorption by the dye results in fast electron transfer to the metal oxide followed by electron transport to the electrode ( $\text{SnO}_2$ ). Dye regeneration occurs through the electron transfer from the liquid electrolyte. DSSC possess the highest conversion efficiency (up to 11%) among organic and hybrid PVs [9,13]. The major factor contributing to the enhanced efficiency is the highly mobile ions in the liquid electrolyte which rapidly compensates the Coulomb interaction between photogenerated electron-hole pairs and thus minimizing the recombination process at the interface. At the same time, the liquid electrolyte is the serious drawback of DSSCs, making them problematic for future technology transition. Attempts to employ solid electrolytes were not very successful and so far the highest reported conversion efficiency for solid DSSC is only 4.5% [14].

Another class of hybrid PVs as shown in Figure 1 is similar to DSSC because of the same nanoporous metal-oxide inorganic matrixes (e.g.,  $\text{TiO}_2$ ,  $\text{ZnO}_2$ ) incorporated in the device architecture. However, instead of employing dye or electrolyte, conjugated polymers (e.g., polythiophene derivatives [10,12], or thiophene-fluorene copolymers [10,15]) function as the organic counterpart. It was previously envisioned that such organic-inorganic system should be very efficient for charge separation and carrier transport due to the large interfacial area between the nanoporous metal oxide

and the infiltrated polymer, as well as the relatively high carrier mobility in polythiophenes ( $\sim 0.1 \text{ cm}^2 \text{ V}^{-1} \text{ s}^{-1}$  [16]). Electron mobility in metal oxide semiconductors is significantly higher (e.g.,  $\sim 440 \text{ cm}^2 \text{ V}^{-1} \text{ s}^{-1}$  for ZnO [17]) than in organic systems. However, reported conversion efficiency to date for these hybrid PVs are relatively low ( $\sim 0.1\text{--}0.6\%$ ), which could be associated with the high recombination rate at the interface (in contrast to DSSC) and the twisted conformation of polymers inside the nanopores, leading to the reduction of hole mobility [10,12,18]. An interesting theoretical model describing the factors limiting the efficiency of organic solar cells (hybrid metal-oxide/organic PVs were included) was reported by Nelson *et al.* [19]. Note, that for metal oxide based hybrid PVs, only the dye or the polymer component contributes to the photoconversion process while the inorganic component provides the interface for charge separation and photocarrier transportation. Because of the wide band gap ( $\text{TiO}_2 \sim 3.1 \text{ eV}$ ;  $\text{ZnO} \sim 3.4 \text{ eV}$ ), metal oxide semiconductors cannot absorb solar light at lower spectral energy.

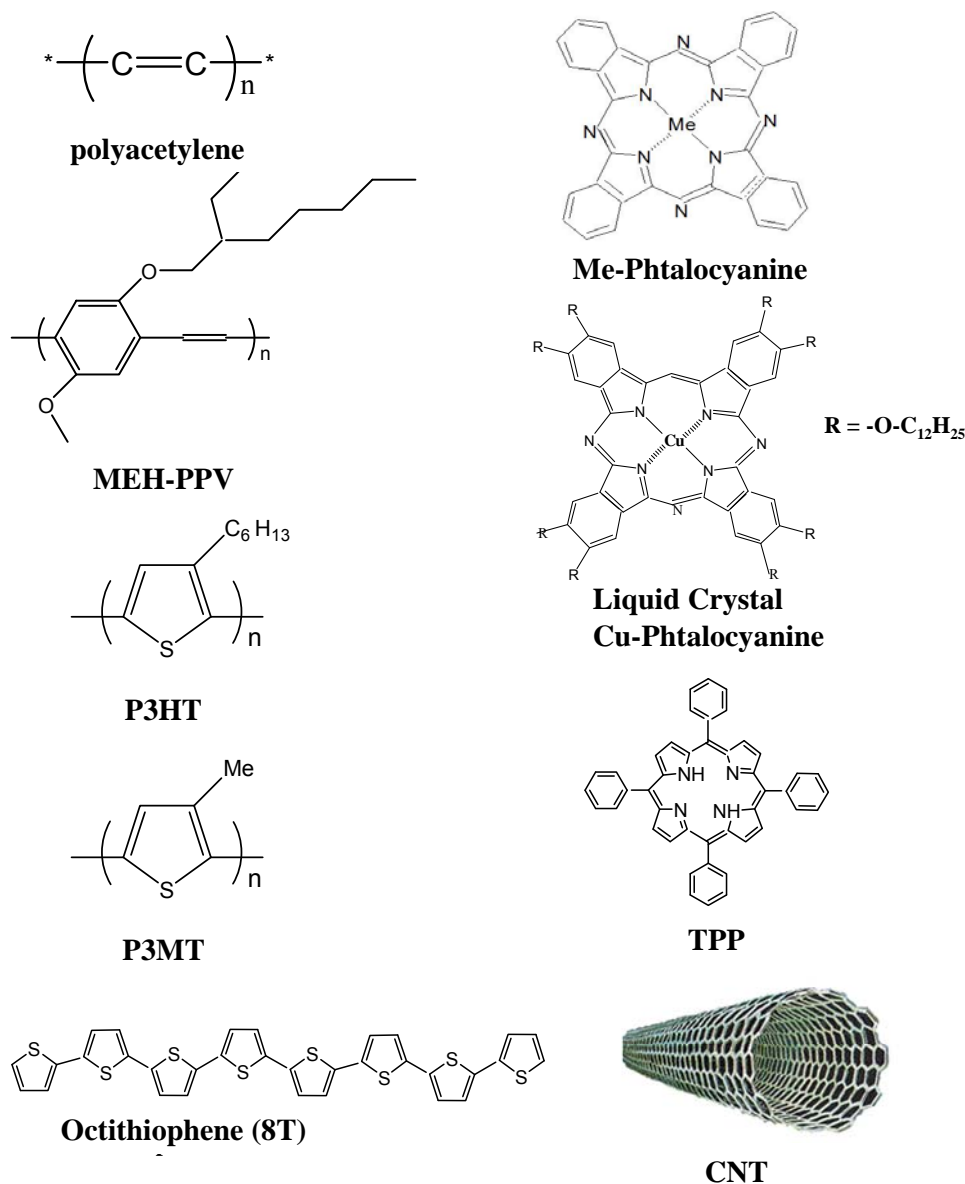
Hybrid PVs based on inorganic nanoparticles (mostly Group II-VI) blended with conjugated polymers (Figure 1) have been considered as a promising nanocomposite photosensitive materials for the past decade [20]. High charge mobility in semiconducting colloidal nano-objects, contribution to the solar light absorption (as distinct from the metal oxides based solar cells), bulk heterojunction and easy wet processing could provide advantages over other hybrid and organic PVs. Nevertheless, their conversion efficiency remains low in the range of 1–3%. The main reasons likely are the electrically inactive network of colloidal nanoparticles/nanorods and the high interfacial recombination rate.

## 2. Hybrid Solar Cells Based on Flat Heterojunction Between Group IV, III-V Semiconductors and Organics

### 2.1. Semiconductor—polymer solar cells

One of the first studies of Si-polymer solar cells was reported by Lewis *et al.* [21], describing a device prepared by coating of poly-( $\text{CH}_3$ )<sub>3</sub>Si-cyclooctatetracene over crystalline Si surface with reported conversion efficiency between 1% and 5%. The role of the polymer in the device design was dual: providing an interface with *n*-type Si (*n*Si) for photocarriers separation and hole collection through the polymer film to the external electrode. The polymer was doped with iodine vapors to enhance the film conductivity. After doping, the polymer became relatively transparent to solar light, thus only Si was involved in photocarrier generations. The achieved photovoltage ( $V_{oc} = 0.64 \text{ V}$ ) was in good agreement with theoretical calculations made for the case of negligibly low interfacial recombination. The control device (Au/*n*Si-Schottky cell) showed  $V_{oc} \sim 0.3 \text{ V}$ , twice lower than the theoretical limit. Historically, the first results about polymer-semiconductors heterojunction for PV applications were reported in 1978 by McDiarmid group [22]. In this work, polyacetylene polymers (*p*-type) were directly grown on an *n*-type ZnS semiconductor wafer. The quantum efficiency spectrum showed a sizable response below the band gap energy (3.7 eV) of ZnS, which was attributed to the polymer contributing to the photoconversion process. The short circuit current was very low (nA range) as a result of the point contact between the electrode wire and the polymer surface.

**Figure 2.** Organic compounds commonly used to interface with Group IV, III-V semiconductors. MEH-PPV is poly(2-methoxy-5-(2-ethyl-hexyloxy)1,4-phenylenevinylene); P3HT is poly (3-hexylthiophene) ; P3MT is poly (3-methylthiophene); TPP is tetraphenyl porphyrin.



Relatively recent studies of Si-polymer hybrids cells, as a rule, dealt with wet coating of conjugated polymers on semiconductor surfaces [23-26]. McGehee *et al.* [23] investigated photovoltaic properties of the heterojunction between amorphous Si (a-Si) and two conjugated polymers, P3HT and MEH-PPV (Figure 2). Amorphous Si is attractive for PV applications because it is inexpensive and can be deposited as a thin film over flexible metal substrates. Based on the photocurrent action spectra, it was found that polymers instead of a-Si provide the major contribution to photoconversion process despite the a-Si absorbing light in the visible/UV range of the solar spectrum. These intriguing results demonstrate the substantial difference between inorganic a-Si solar cells (where a-Si is a photoactive component) and hybrid devices when excitonic effects in polymers dominate over unbound photo electron-hole pairs in amorphous semiconductor. The authors suggested two mechanisms of charge

separation at the a-Si/polymer interface: (i) exciton diffusion toward the interface, its dissociation and electron injection to semiconductor; (ii) Forster like energy transfer from polymer to semiconductor followed by backward hole injection in the polymer. Despite of the interesting approach for the development of cost effective, thin film hybrid photovoltaics, conversion efficiencies were very low, e.g., 0.16% for a-Si/P3HT and 0.01% for a-Si/MEH-PPV devices [23]. Some improvements in the conversion efficiency were attained later by nanostructuring of a-Si surface [24] (see next section). The replacement of amorphous Si with crystalline *n*Si in the similar device with P3HT resulted in considerable enhancement of the conversion efficiency, up to 2.46% ( $60 \text{ mW/cm}^2$ ) [26]. This could be explained by the faster electron mobility, higher absorption in NIR/red spectral range, and lower interfacial recombination in the crystalline Si as compared with amorphous Si.

Another class of hybrid solar cells with flat heterojunctions is GaAs/thiophene based polymers and oligomers [27–30] (Figure 2). The first study of poly (2 methylthiophene) (PMeT)/GaAs based solar cell was reported in 1986 by Horowitz and Garnier [27]. Later, an almost identical result was published by Garnier in 2002 [28]. The top electrode in these devices was a thin Au layer sputtered on the polymer. This circumstance added certain difficulties in interpreting the experimental results because of the PV action for Au/*n*GaAs heterojunction, which is typical for Schottky barrier solar cells. Thus, although the polymer insertion between Au and GaAs could improve the PV performance, which indeed was observed, the real picture of photoconversion process at the presence of the two interfaces (Au/P3HT and P3HT/*n*GaAs) is far from a complete understanding. Despite the authors claiming a conversion efficiency of 17.5% (corrected on Au reflection), the actual values did not exceed 1% for a real Au/P3HT/*n*GaAs based solar cell.

It is interesting that a similar device structure, where the P3HT polymer was replaced by thermally evaporated rod-like octylthiophene (8T) (Figure 2) allows to elucidate the role of the film morphology for efficient photoconversion [29]. Microcrystalline 8T films (deposited at  $140^\circ\text{C}$ , grain size  $1\text{--}2 \mu\text{m}$ ) exhibited much higher conversion efficiency than nanocrystalline 8T films (deposited at  $100^\circ\text{C}$ , grain size  $0.1 \mu\text{m}$ ). It was found that microcrystalline films provides better ordering of 8T oligomers leading to the exciton diffusion length of several tens nanometers, while nanocrystalline film with low ordering clearly demonstrated photocurrent losses presumably owing to the higher trap density (mostly at the grain border). The best conversion efficiency for a Au/8T/*n*GaAs cell was 4.2%, corresponding to an organic layer thickness of 20 nm. However, the power intensity was only  $60 \text{ mW/cm}^2$  and the Au layer was doped with iodine vapors in order to increase the electrode conductivity. In contrast to study [27] (where PMeT was photo-inactive), 8T layer definitely contributed to the photoconversion process.

## 2.2. Semiconductor—small molecules solar cells

The use of organic small molecules to form heterojunctions with semiconductors (mostly Si) for hybrid PVs has been intensively studied for the past decade. In solar cell design, small molecules could have advantages over polymers due to the higher molecular ordering (quasi-crystalline/crystalline structure) and better environmental stability. In the crystal phase, charge mobility ( $\sim 0.2 \text{ cm}^2\text{V}^{-1}\text{s}^{-1}$  [31]) can be comparable or even exceed the carrier mobility in polythiophene based polymers ( $\sim 0.1 \text{ cm}^2\text{V}^{-1}\text{s}^{-1}$  [16]). The physical and chemical properties of organic molecules selected should satisfy at least two major conditions: high absorption coefficient in the solar spectrum

and sufficient electrical conductivity in the solid state. A various derivatives of phtalocyanines (Pc) and porphyrines (Ph) can be considered as promising candidates for the construction of the heterojunction with semiconductors (Figure 2). Phtalocyanines and porphyrines (especially metal substituted Pc (MePc)) have been well studied for molecular optoelectronic and electrophotography applications. Pc and Ph demonstrated an excellent photoconductivity that allows for utilizing in the design of various organic solar cells and photodetectors. Therefore, most of the reported studies of semiconductor-small molecules hybrid cells are related to Pc and Ph compounds. In particular, *p*Si/CuPc [32], Si/ZnPc [33,34], *n*Si/MgPc [35], *p*Si/NiPc [36], *n*GaAs/CuPc [37] and *n*Si/TTP [38] (Figure 2) hybrid solar cells were reported in literature with conversion efficiencies in the range of 1–3.5%. An additional advantage of phtalocyanines is their exceptional chemical stability. However, for film deposition, the major amount of Pc and Ph compounds requires vacuum sublimation due to the low solubility in organic solvents and water (except derivatives with long alkyloxy chains). This circumstance is a serious drawback making it impossible to apply the simple and cost effective wet processing for hybrid cell fabrication.

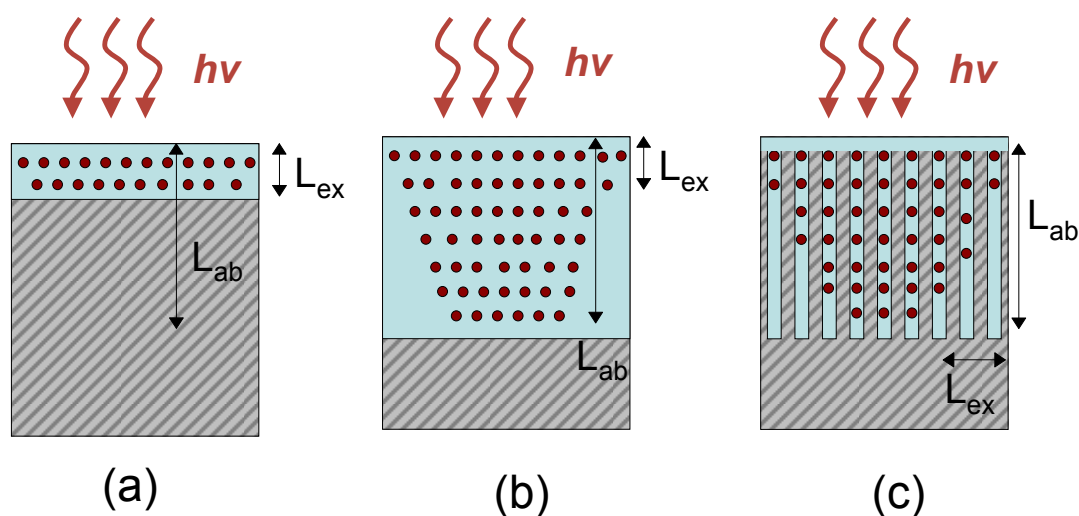
The physics of photovoltaic effect is far from a full understanding in terms of photocarrier generation and separation. Surprisingly, none of these studies presented photocurrent action spectra. Therefore, it is difficult to estimate the contribution of Si and organic component to the light absorption and photoconversion. Only in study [35], the photocurrent spectrum of *n*Si/MgPc device was detected, and matches well with the optical absorption of MgPc. This is indicative of the dominating role of organic layer in the photoconversion process (note that the minimal thickness of MgPc film was 170 nm, which could be sufficient to block the light for Si component). The analysis of the optoelectronic properties for all of the above-mentioned diodes were based on *p-n* heterojunction models applicable for inorganic semiconductors and neglecting the excitonic origin of photocarriers in organic component. Despite such limitations, several important parameters were extracted from the analysis of *I-V* and *C-V* characteristics. In particular, in almost all types of devices, it was found that the predominant current mechanism (in forward direction) is trap assisted multistep tunneling. Also, all of the solar cells demonstrated better PV performance than the control device (Au/Si solar cell) which is indicative of the contribution of excitons generated in organic layer and the reduction of interfacial trap density.

### 3. Hybrid Devices Composed from Nanostructured Semiconductors (Si, GaAs, InP, Ge) and Organics

Recent progress in the nanostructuring of semiconductors opens a new opportunity for improvements in the performance of hybrid solar cells. First of all, the quantum confinement dramatically changes the opto-electronic properties of nanostructured semiconductor leading to the tunable band gap, enhancement of the light absorption, and altered electrical conductivity depending on the characteristic size at nanoscale environment. Such circumstance provides an additional parameter (nanoscale tunability) for optimal compatibility between the organic and the inorganic components in order to form heterojunctions with advanced PV characteristics. The morphology of the heterojunction is also important as such devices have increased interfacial area and reduced average distance from one point to an interface. As the separation of charge carriers occurs at interfaces

through exciton dissociation, such structures enhance it, and thus lead to an increase in the photocurrent. Figure 3 presents the schematic demonstrating potential advantages of nanostructured organic-inorganic interface over flat heterojunction. In terms of the efficiency of the organic layer in the case of a flat heterojunction, the figure of merit can be formulated as  $F \sim L_{\text{ex}}/L_{\text{ab}}$ , where  $L_{\text{ex}}$  is the exciton diffusion length and  $L_{\text{ab}} = 1/k$  is the light penetration length ( $k$  is the absorption coefficient). Thus, thin organic layer with thickness of  $d \sim L_{\text{ex}}$  and  $d < L_{\text{ab}}$ , provides efficient charge separations (all excitons reach the interface) but low absorbance (Figure 3a). In contrary, relatively thick organic layer ( $L_{\text{ab}} \sim d > L_{\text{ex}}$ ) absorbs more light energy, but only a fraction of the excitons are capable of dissociating at the interface (Figure 3b). In the case of nanostructured semiconductor infiltrated with organics, the characteristic length (average distance between pillars or pore diameter) can be comparable with the exciton diffusion length, while the nanostructured layer can be thick enough to absorb substantial light energy (Figure 3c). However, it should be noted that the large interface increases interfacial recombination. As a rule, for many polymers and small molecules,  $L_{\text{ex}}$  (several tens nm for singlet excitons) is lower than  $L_{\text{ab}}$  of several hundreds nm. Therefore, an optimal design of nanostructured semiconductor could comprise of axial nanoobjects such as pillars or pores (better ordered) with an average distance  $\sim 5\text{--}20$  nm and length of 500–1,000 nm or longer.

**Figure 3.** Exciton (dots) generation in the hybrid structures with flat (a,b) and nanostructured heterojunction (c).



### 3.1. Nanowires and nanopillars

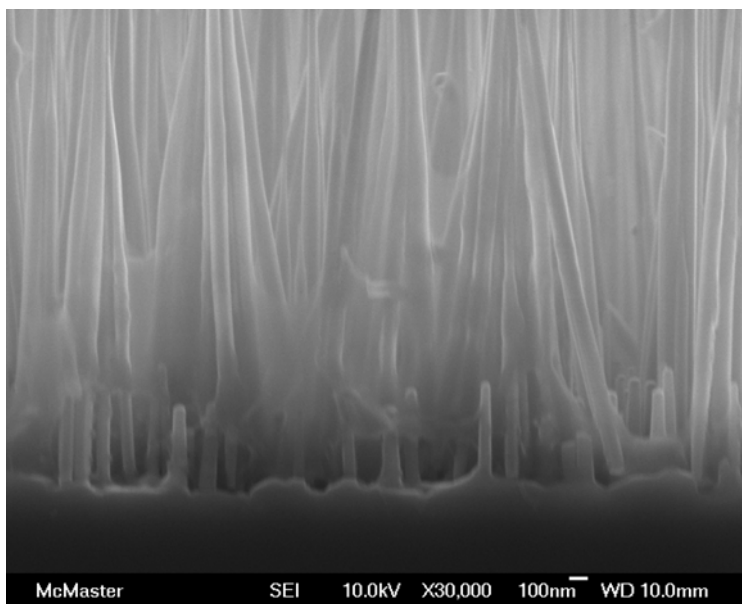
Recently, a new trend in hybrid photovoltaics emerges as a result of intensive efforts in the field of nanowires/nanopillars growth from Group IV, III-V semiconductors. These nanostructures provides a large interfacial surface in contact with the organic materials and can be easily fabricated by various techniques such as chemical vapor deposition (CVD) [43], laser ablation [41], molecular beam epitaxy (MBE) [42], dry etching [24]. Hybrid solar cells based on Si [39–41], GaAs [42], InP [43], Ge [44] nanowires (NW) and polymers (mostly P3HT) has been reported in literature for the last 2–3 years.

Figure 4 shows the cross-sectional SEM image of ordered GaAs nanowires grown on  $n$ -type GaAs substrate after infiltration with P3HT polymer [42]. The conversion efficiency of the cell with ITO/P3HT-NW/GaAs/Me structure can be varied from  $<0.1\%$  to  $1.04\%$  (2.6 sun) depending on the



P3HT solvent composition and the nanowire etching time (prior to deposition to remove the native oxide). The control devices (nanowires without P3HT and P3HT without nanowires) demonstrated negligible PV response, which is indicative of the importance of the nanostructured interface in the device architecture.

**Figure 4.** Cross-sectional image of GaAs nanowires infiltrated with P3HT [42]. Reproduced with permission from the Institute of Physics and IOP Publishing Limited, ©2009.



PV response of Si nanowires-P3HT interface has been investigated in study [39]. The NWs of smaller sizes (3–5 nm) resulted in higher open-circuit voltage and higher short circuit current than nanowires with larger diameters (10–20 nm) [39]. The authors suggested that a widening of the band gap for smaller NWs decreases the conduction band offset between the Si NW and the P3HT leading to reduced voltage loss during exciton dissociation. The highest conversion efficiency was 1.15% (1 sun) for Si NWs with diameters of 3–5 nm and 35 wt% ratio of NW to P3HT. In study [41], the Si NWs were fabricated by etching process. Then, the NWs were pressed into P3HT layer followed by removal of the wafer. The reported conversion efficiency of such device was 1.93%. In both studies [39,41], the Si NWs definitely contributed in the photoconversion process by light harvesting in the NIR range, where the polymer cannot absorb light energy.

A novel approach in the design of hybrid solar cells has been described in Ref. [43], where InP nanowires were directly grown on ITO substrate. It was shown that Ohmic contacts were formed between the NWs and the ITO layer, which is a substantial achievement compared to NW/polymer blend sandwiched between two electrodes. In this case, the NWs provide a direct pathway for electron transport and collection at the ITO electrode. PV response was improved by the passivation of the InP surface with sulfur, which reduces nonradiative recombination. However, the conversion efficiency was low (<0.1%), likely because of the thick non-uniform P3HT (4–6  $\mu\text{m}$ ) layer prepared by drop casting. At such thicknesses, charge transport through the polymer network cannot supply enough holes to the external electrode due to low hole mobility and hole trapping ( $L_{\text{ab}} \sim d > L_{\text{ex}}$ , Figure 3b).

Nanostructured surface of amorphous Si (a-Si), prepared by nanosphere lithography and reactive ion etching, resulted in an improvement of the PV response for ITO/nanostructured a-Si/P3HT/Ag device [24]. Such nanostructure can be presented as interconnected array of nanopillars with average pore sizes of 30–40 nm. The conversion efficiency was increased up to 0.3% as compared with flat heterojunctions (0.16%) [23]. The higher pillar height leads to enhancement of the short circuit current and is likely associated with an increase of the surface interface between P3HT and a-Si.

### 3.2. Nanoporous wet etched structures

An alternative approach to nanowire growth is the use of nanoporous semiconductors fabricated by electrochemical etching process (mostly porous Si, however porous GaAs and other III-V semiconductors were also investigated [45]). The electrochemical etching of Si is a well known technique for preparation of various porous structures with pore sizes from ~5–50 nm (mesoporous) to several hundreds nanometers (macroporous) [46]. There are only a few reports about hybrid cells based on mesoporous Si infiltrated with small molecules [47–49], however this fabrication method is simple (wet processing as distinct from nanowire growth) and can obtain conversion efficiencies up to ~3% [48], exceeding those of nanowire based hybrid PVs [39–44].

In study [47], mesoporous *n*-type Si (PSi) was infiltrated with CuPC and its derivative discotic liquid crystal CuPCL (CuPCL) (Figure 2). The choice of CuPCL was motivated by the possibility of increasing the hole mobility along the quasi-1D columns, similar to LC perylene derivatives [31]. It was shown by A. Komolov *et al.* [50] that electron transfers from CuPC film to *n*-Si (100) substrates extends a positively charged layer into the CuPC film up to 10 nm. Porous Si has several important functions in hybrid solar cells. It serves as light absorber, antireflection coating and as nanostructured material for electron transfer and transport. The CuPC provides the light absorption, charge separation at the interface with PSi and hole transport medium. Figure 5 shows the SEM image of PSi prior to and after infiltration with CuPC.

Contrary to anticipations, CuPCL based cells demonstrated significantly lower conversion efficiency, ~0.01% (comparable with the control device—the same cell without organic components) than solar cells infiltrated with CuPC with efficiencies up to 3%. Such striking differences can be explained in terms of the interfacial area between the organic and the inorganic components. Presumably, the electron transfer from CuPCL to Si is slow enough or is nonexistent due to relatively long alkyloxy chains (Figure 2), which could prevent close contact of the CuPCL molecular core with PSi. Thus, the critical issue becomes an average distance between a CuPC core to the PSi surface and LC organization cannot compensate the low photoinduced electron transfer caused by the long alkyloxy chains.

**Figure 5.** (a) SEM image of Si surface and cross-section after electrochemical etching: 15% HF/ethanol solution, 20 s, 50 mA/cm<sup>2</sup>, the porous layer depth is 1,400 nm. (b) The same sample after infiltration with CuPC/H<sub>2</sub>SO<sub>4</sub> (cross-section only) [48]. Reproduced with permission from SPIE, ©2005.

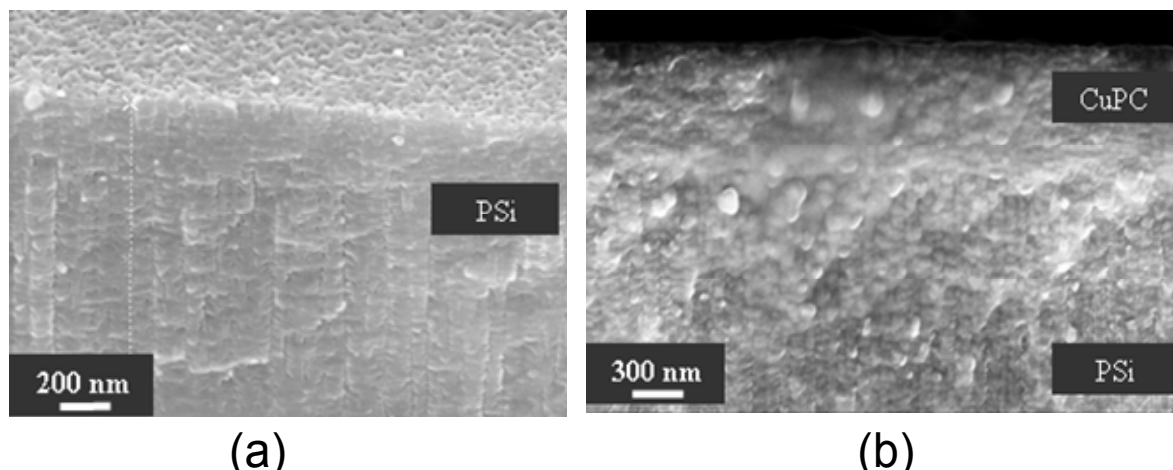
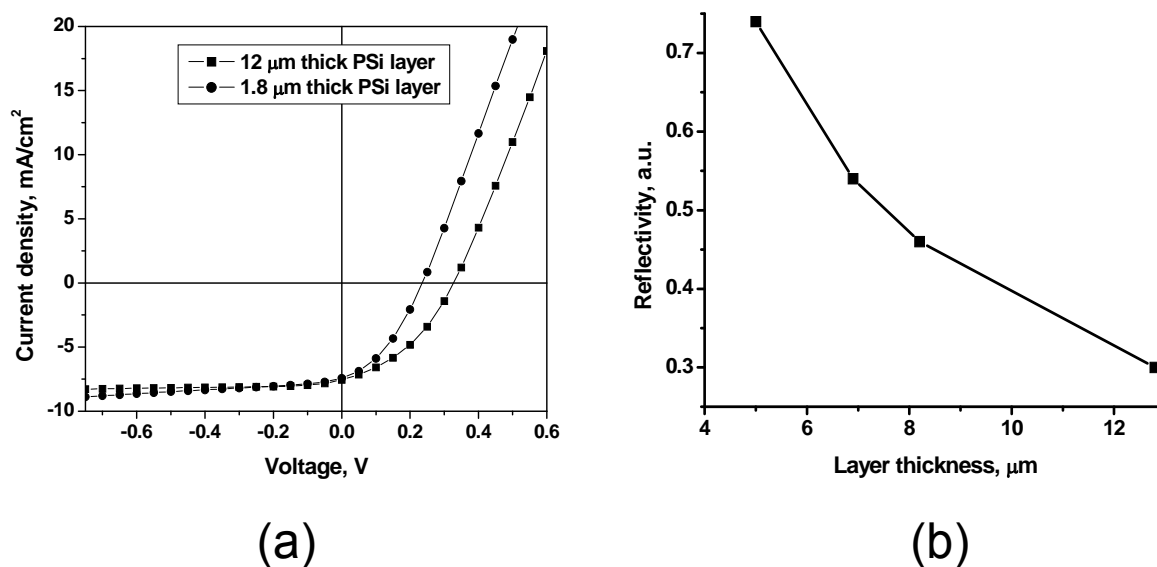


**Figure 6.** (a) *I-V* characteristics of the ITO/PSi-CuPC/Si/Cr/Au cells with different thicknesses of PSi layer at white light illumination (33 mW/cm<sup>2</sup>): Circles: PSi layer thickness is 1.8  $\mu$ m:  $I_{sc} = 7.40$  mA/cm<sup>2</sup>,  $V_{oc} = 0.237$  V, FF = 29%,  $\eta = 1.6\%$ ; Squares: PSi layer depth is 12  $\mu$ m ( $I_{sc} = 7.56$  mA/cm<sup>2</sup>,  $V_{oc} = 0.325$  V, FF = 40%,  $\eta = 3\%$ ). (b) The dependence of reflectivity of PSi layer with porosity 35% on its thickness at 650 nm [48]. Reproduced with permission from SPIE, ©2005.

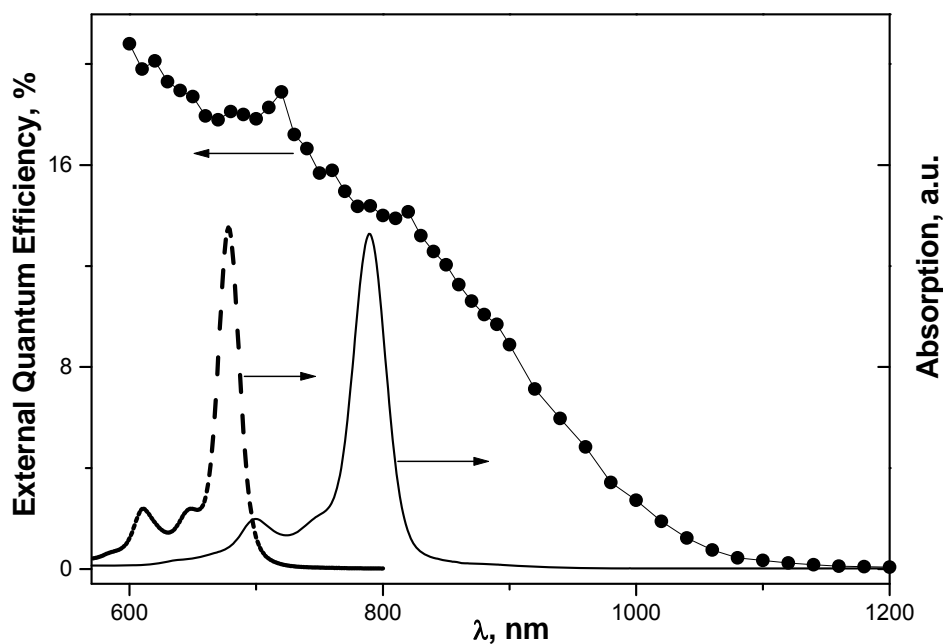


In addition, the effect of porosity and layer thickness on PV performance was investigated [48]. The *I-V* characteristics are shown in Figure 6a for two devices with different thickness of PSi layer. The conversion efficiency was enhanced from 1.6% to 3% with an increase of the pore depth from 1.8  $\mu$ m to 12  $\mu$ m. At the same time, the reflectivity drops from 80 % to 30%, measured at 650 nm (Figure 6b). Thus, an increase of the conversion efficiency is most likely a result of reduced reflectivity of the deeper porous layer. An efficient penetration depth of CuPC is about 200 nm according to XPS data,

which is indicative of potential for the following improvements of PV properties using deep and uniform filling.

Two PSi samples with similar reflectance spectra but with different porosity (35% and 75%) were employed to fabricate PV devices. It was found that the sample with lower porosity (35%) exhibits higher conversion efficiency by an order of magnitude than the sample with higher porosity (75%). Hence, the Si porosity plays a key role in the carrier transport, affecting the device performance [48]. According to study [51], as crystalline Si becomes porous, conductivity decreases because of the strong dependence of the diffusion coefficient on the porosity value. When the porosity reaches 57%, the conductivity of the PSi is dramatically reduced. This implies that the conductivity in PSi with porosity higher than 57% is determined by a hopping mechanism between crystallites. Thus, an ideal structure of the PSi layer for PV applications could be a low porous layer with sufficient thickness of  $\sim 10\ \mu\text{m}$  and higher.

**Figure 7.** External quantum efficiency of the Au/Psi-CuPC/Si/Al cell. Absorption spectra of CuPC in concentrated  $\text{H}_2\text{SO}_4$  solution (solid line) and CuPC1 in chloroform solution (dashed line). Concentration is  $10^{-5}\ \text{M}$ . Shift of CuPC spectrum with respect to CuPC1 spectrum is the result of CuPC protonation in  $\text{H}_2\text{SO}_4$  solution. Reprinted with permission from [47]. Copyright [2004], American Institute of Physics.



The contribution of CuPC to PV effect can be seen in the spectral dependence of external conversion efficiency, which exhibits two peaks (720 and 820 nm) matching the absorption bands of the protonated CuPC form in  $\text{H}_2\text{SO}_4$  solution (Figure 7). The long wavelength edge of the spectrum corresponds to the band gap of Si (1.1 eV) but not porous Si ( $\sim 2\ \text{eV}$ ). Hence, the absorbance of the porous layer is low or the porosity in the *n*-type Si is not sufficient to change the band gap.

The similar dependence of the conversion efficiency on the porosity layer has been observed in study [49], where the device with porosity of 24% demonstrated an efficiency of 1.2% in contrast with the 0.91% value for the device with porosity of 62%. The authors suggested that such effect is

associated with the increased distance between CuPC and PSi surface for highly porous structure. However, a more plausible explanation is related to the abrupt conductivity reduction for porosities more than 57% [51].

#### 4. Solar Cells Based on Silicon and Carbon Nanotubes

Despite significant achievements for the past decade, hybrid PVs from Group IV, III-V semiconductors and organics (polymer and small molecules) still remain promising objects for future research. Their conversion efficiency so far does not exceed the level of 3–4%, which is not sufficient for any commercial applications. This situation however can soon be dramatically changed, as a result of recent research related to PV properties of CNTs—Si heterojunction [52–56].

It is known that the major drawback of hybrid solar cells is insufficient PV quality of the organic component, which is attributed to the low charge mobility, lack of absorbance in the red/NIR spectral range, and chemical instability. On the other hand, the obvious advantages of organics are wet processings, light weight and flexibility.

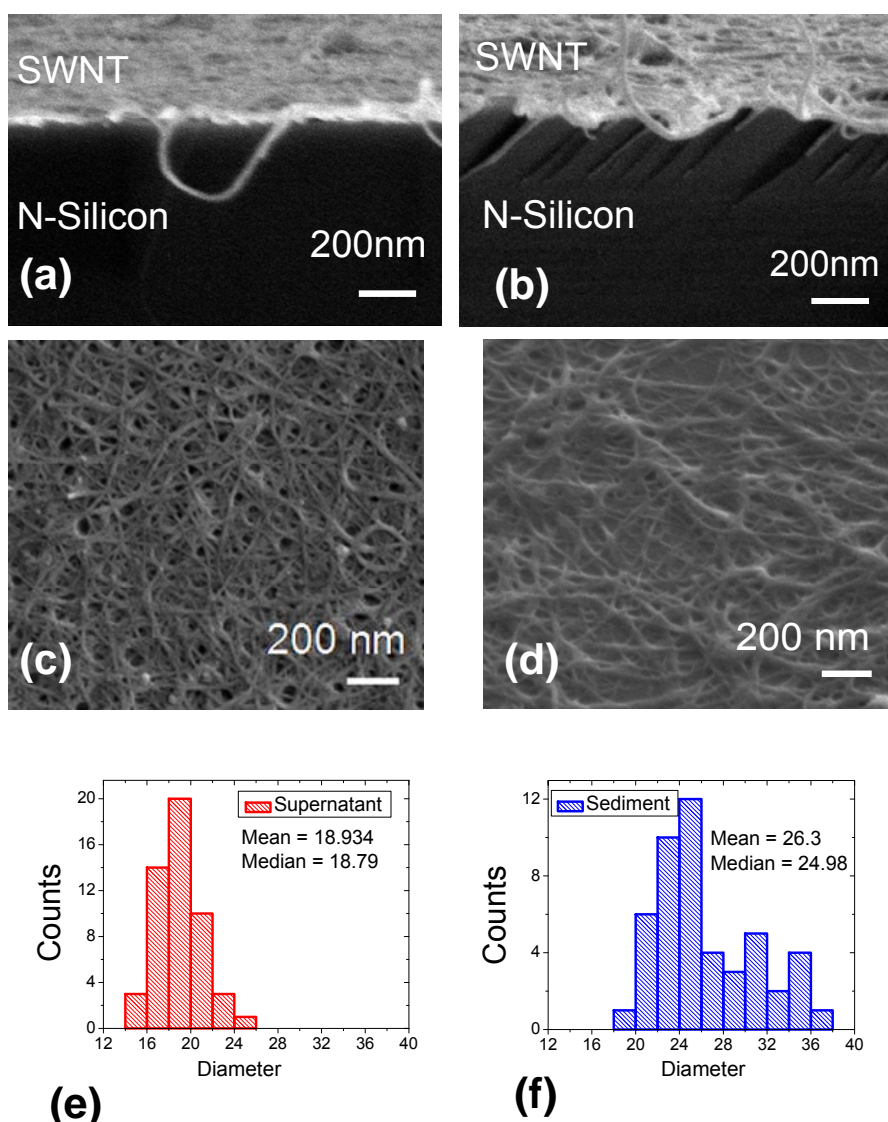
Remarkably, CNTs possess the above-mentioned advantage and are free from the mentioned deficiency. Indeed, the unique optoelectronic properties of CNTs [57] make them a favorite candidate compared to other organic materials for incorporating in the structure of hybrid solar cells. First, CNT charge mobility can be up to  $10^5 \text{ cm}^2\text{V}^{-1}\text{s}^{-1}$  for individual nanotubes [58] and  $\sim 60 \text{ cm}^2\text{V}^{-1}\text{s}^{-1}$  for CNT films [59], which is much higher than the hole mobility in P3HT polymer (one of the best organic conductor). Second, CNTs has a high light absorbance in the red and NIR spectrum (absorbance coefficient of  $10^{-4}$ – $10^{-5} \text{ cm}^{-1}$ ). Third, they exhibit an exceptional environmental stability. Fourth, carbon nanotubes can be deposited easily to the semiconductor surface by wet processing techniques (coating, spraying, and printing). Finally, CNTs can be easily doped or functionalized, thus tuning the Fermi level to the favorable position when forming heterojunction with semiconductors [60–62].

The photoconductive response of films prepared from single walled carbon nanotube (SWNT) under laser pulse excitation was first reported by Fujiwara *et al.* [63]. Subsequently, photocurrent response of SWNT film under continuous wave illumination were reported by Levitsky *et al.* (SWNT films) [64] and for individual SWNT bundle by Freitag *et al.* [65]. It is important that the combination of CNTs of varying diameters and chiralities, and correspondingly different band gap (the band gap is inversely proportional to diameters) makes it theoretically possible to obtain a continuous photoresponse over a broad spectral range covering the red and NIR part of the solar spectrum.

For the past decade, applications of CNTs in organic solar cells were mostly focused as nanoscale fillers for polymer films [66–71]. The donor-acceptor configuration, where the high aspect ratio and large surface area of nanotubes incorporated in these polymers was believed to be favorable for higher exciton dissociation and increased charge carrier transport. However, the power conversion efficiency for these structures remains relatively low (<1%) possibly due to the low carrier mobility in polymers and poor dispersion of CNTs in polymer matrix. Another way to employ CNTs in solar cell design is the use of CNTs as a transparent conductive coating to replace metal oxides electrodes (e.g., ITO) for organic PVs [62,73]. Nevertheless, little progress has been achieved in this direction as the conductivity of the CNT network is still lower than the conductivity of ITO at the same transparency level in the visible spectral range.

Very recently several groups reported the hybrid solar cells based on heterojunction of CNTs and *n*-type Si [52–56] where CNTs function as active photosensing component being involved in the light absorption, charge separation and charge transport. Surprisingly, only for the past two years, the conversion efficiency of such devices exceed the level of 7% [54] and are very promising for even higher conversion efficiency with special CNTs treatments and device optimizations.

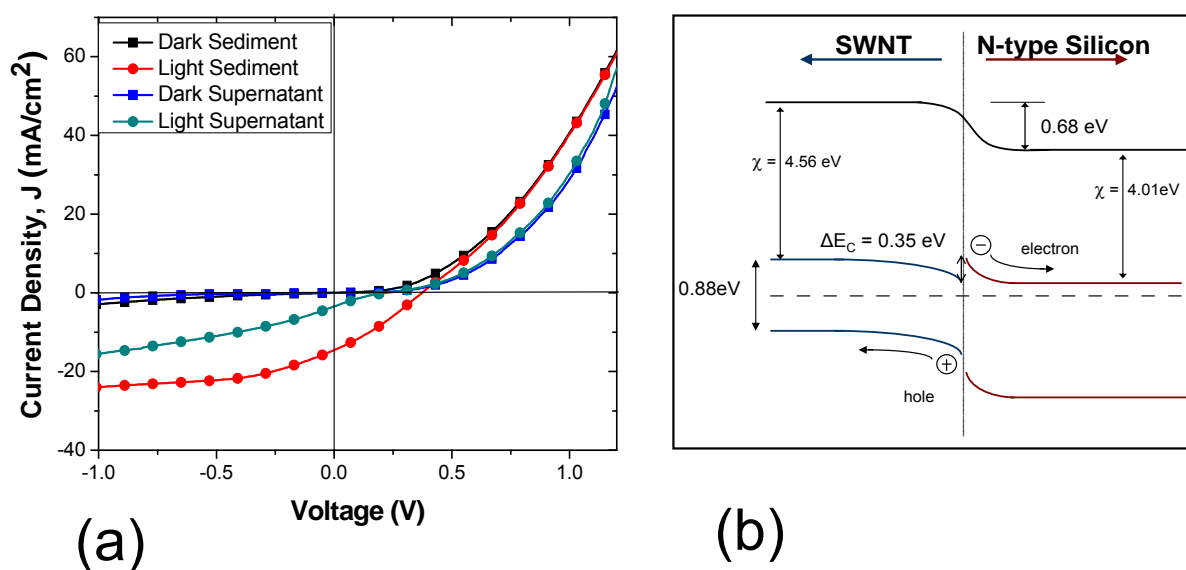
**Figure 8.** SEM images (a–d) of SWNT films deposited on a *n*-type Si by spraying technique from supernatant and sediment fractions. Cross-sectional view of (a) supernatant and (b) sediment. Top view of (c) supernatant, and (d) sediment. Diameter distribution histogram of SWNT bundles for (e) supernatant and (f) sediment. From the SEM images and histogram, sediment sample shows thicker and longer SWNT bundles compared to supernatant [56]. Reproduced with permission from Institute of Physics and IOP Publishing Limited, ©2009.



The hybrid *n*Si/CNTs solar cells are comprised of a thin layer of nanotube films, deposited either via air-brush spraying of nanotube suspension [52,53,56] or lift-off wet deposition process [54,55] on *n*-type silicon wafers. The morphology of these films is a network of nanotube bundles (consisting of

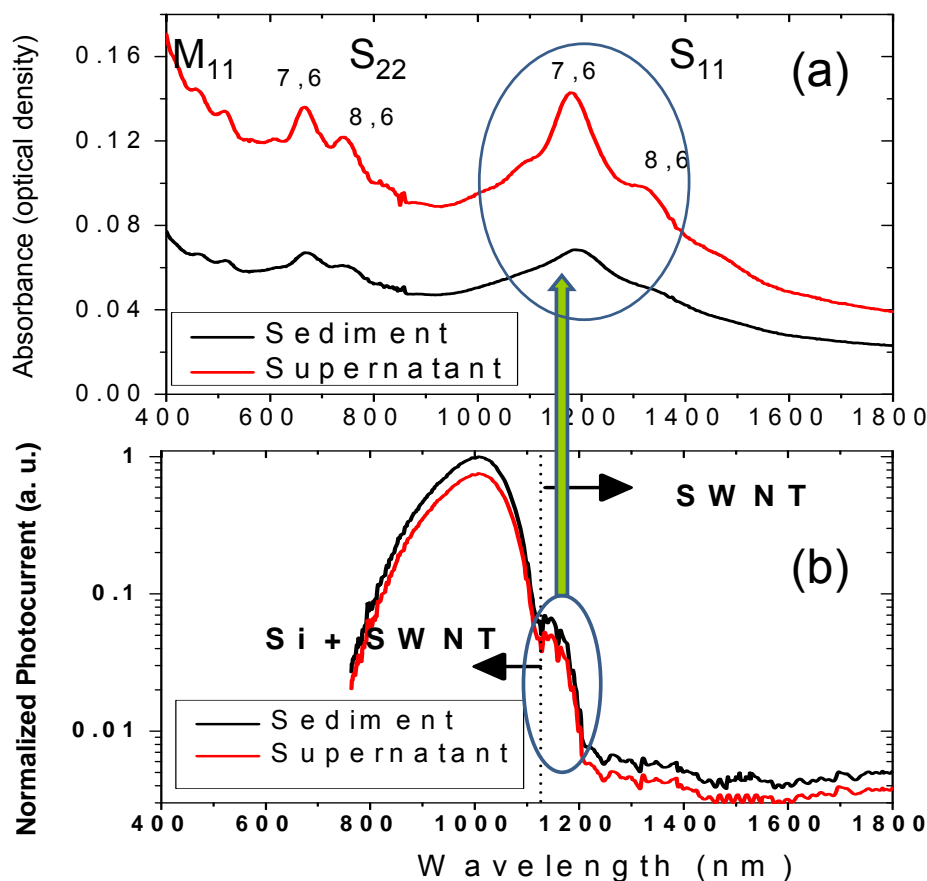
several tens of individual nanotubes) with highly porous structure (Figure 8c,d). Because semiconducting single walled nanotubes (SWNTs) and double walled nanotubes (DWNTs) are naturally *p*-type conductors, when interfaced with *n*-type Si, they form *p-n* heterojunctions. *I-V* measurements of *n*Si/SWNT heterojunction [56] exhibit typical solar cell characteristics under dark and under light illumination (Figure 9a). Such rectifying behavior can be explained by the schematic energy band diagram based on Anderson model as shown in Figure 9b. As shown in the band diagram, a large built in electric field is formed at the interface. The source of photocarriers in SWNTs is excitons with a binding energy  $\sim 0.4$  eV [74], which are dissociated at the interface due to the built-in field. It is likely that the electrons then tunnel to the Si layer and holes are transported through the SWNT network to the external electrode. Photogenerated free carriers in Si can also be separated at the interface followed by photohole injection from Si to SWNTs.

**Figure 9.** (a) Current-Voltage (*I-V*) plot of sediment and supernatant SWNT/*n*Si devices under dark and light illumination. (b) Schematic energy band diagram of SWNT/*n*Si heterojunction based on the Anderson model. Electron affinity,  $\chi$  and conduction band offset,  $\Delta E_c$  for SWNT and *n*Si are shown in the energy band diagram [56]. Reproduced with permission from Institute of Physics and IOP Publishing Limited, ©2009.



The role of SWNTs in photoconversion efficiency of the hybrid cell was not clearly understood in studies [52,53,55] as no photocurrent action spectra were recorded. The first measurement of photocurrent spectra showed maximum quantum efficiency peak at 1.2 eV, which is close to the energy gap of Si (1.12 eV) [54], however a low resolution did not allow to identify the possible band responsible for DWNT absorption and photoconversion. Later, Levitsky *et al.* [56] demonstrated a matching photocurrent band of the *n*Si/SWNT device to the first transition band of the NIR absorption spectra of the SWNT film (Figure 10). Thus, the CNTs in the hybrid *n*Si/CNT heterojunction solar cells contribute to the photo conversion process not only as a charge separator/transporter/collector but also as a light absorber. This is an important fact, distinguishing between a heterojunction solar cell with two active light absorbing components and a Schottky cell, where the metal component is not capable of absorbing photons.

**Figure 10.** (a) UV-Vis NIR spectrum of sediment and supernatant fraction from centrifugation process of SWNT films on glass with sheet resistance of 1 k $\Omega$ /square.  $M_{11}$ ,  $S_{22}$ , and  $S_{11}$  represents the band-gap transitions in metallic and semiconducting SWNTs. (b) Normalized photocurrent spectra (area and intensity of light source) of the solar cell devices (supernatant and sediment) showing a current peak band (due to SWNT) matching the  $S_{11}$  band [56]. Reproduced with permission from Institute of Physics and IOP Publishing Limited, ©2009.



Although, the conversion efficiency of  $n$ Si/CNT solar cells is still lower than that of conventional Si cells, there are several methods currently explored to increase the PV performance through CNT doping, functionalizing and separation. SWNT chemical modification by thionyl chloride allowed to increase the conversion efficiency by more than 50% reaching the value above 4% [53]. Another approach, using high speed centrifugation, has been applied to separate SWNTs on high (sediment) and low (supernatant) conductive fractions [56]. Figure 8 shows the SEM images and diameter distribution for SWNT film on Si surface deposited by spraying from sediment (SD) and supernatant (ST) fractions. SD based cells demonstrated an efficiency ( $\sim 1.7\%$ ) higher by a factor of  $\sim 8$  as compared with ST cells ( $\sim 0.2\%$ ) and by a factor of 2 as compared with sonication only based solar cells ( $\sim 0.8\%$ ), where SWNT were sprayed without centrifugation [56].

All of the above promising findings allow us to believe that PV performance of hybrid  $n$ Si/CNT solar cells could be further substantially improved to overcome the 10% threshold of conversion efficiency needed for commercial applications.

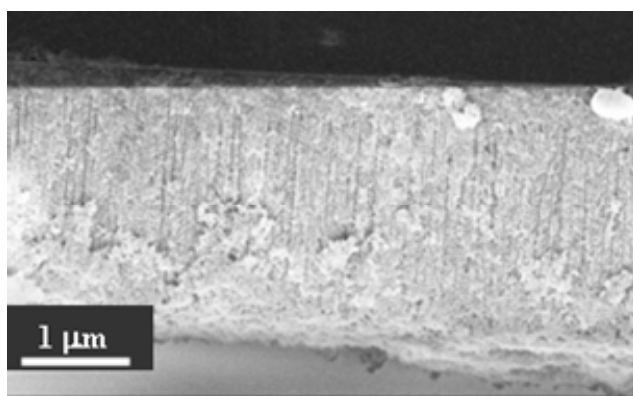


## 5. Summary and Strategies to Improve PV Performance of Hybrid Solar Cells

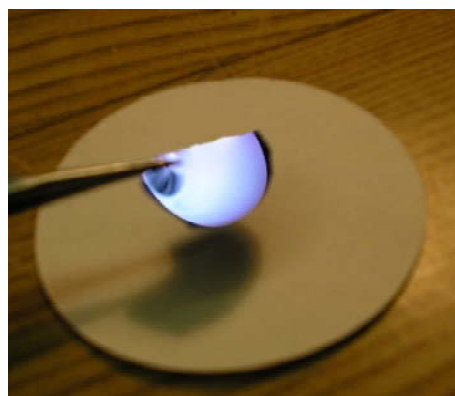
Much progress for the past decade has been made towards making hybrid solar cells with advanced PV properties. Up until recent years, pure organic PVs led in competition with hybrid devices, demonstrating higher efficiency (up to 6.5% [5]) over 3–4% for various organic-inorganic structures. However, it seems that organic P3HT: PCBM (or CuPC: C60) based devices have already exhausted their potential as no significant progress were achieved for the past two years. Contrary, an efficiency of 7.4% [54] which was reported in 2008 for hybrid Si/CNTs based solar cells opened new opportunities to overcome the critical barrier of 10% efficiency. This finding and other promising recent results [52,53,55,56] suggest to revisit the role of Si and Group III-V semiconductors as inorganic component for hybrid PVs that currently employ mostly metal oxides and II-VI semiconductors.

Silicon (the most widely used semiconductor in solar cell industry) can be easily integrated in the hybrid cell design, not only as a crystalline component but also as microcrystalline, amorphous and porous structure. Non-crystalline Si still maintains high charge mobility exceeding mobilities of most organic compounds. At the same time, Si can be prepared as thin films by CVD (amorphous Si) or electrochemical etching (mesoporous Si membrane). Figure 11 shows the SEM and photo images of lightweight mesoporous Si membrane. Such membrane infiltrated with polymers can attain an excellent flexibility [75] comparable with many plastic substrates. Furthermore, porous Si allows introducing photonic bandgap structure in the device, reducing reflection and increasing light trapping, which is of utmost importance for thin film PVs.

**Figure 11.** (a) SEM image of the freestanding PSi membrane fabricated in 15% HF/ethanol solution at 50 mA/cm<sup>2</sup> current density and electrochemically separated from the substrate using 250 mA/cm<sup>2</sup> current density [48]. Reproduced with permission from SPIE, ©2005. (b) Photo image demonstrating the PSi membrane fabricated at Emitech, Inc.



(a)

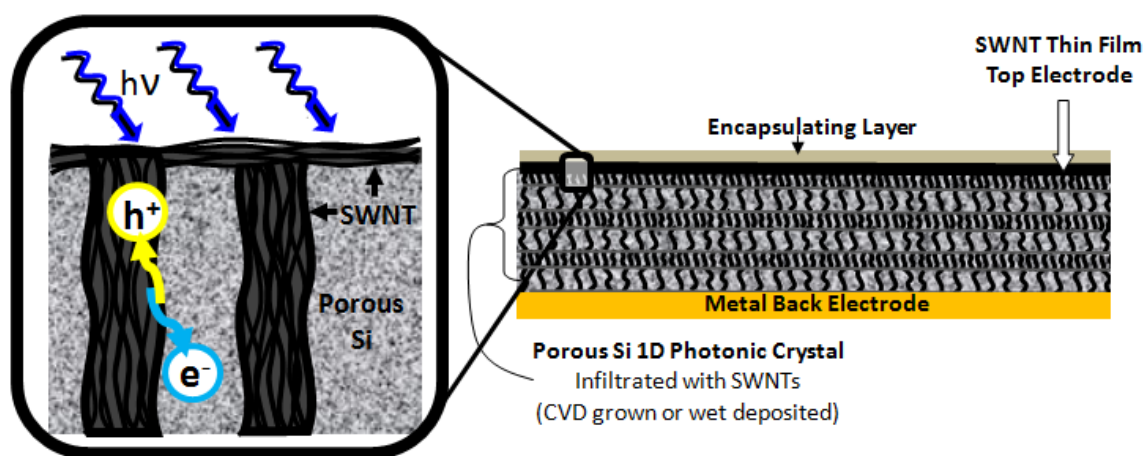


(b)

Developing novel organic materials with high hole mobilities and enhanced light absorbance in the broad spectral range might be the other promising direction to achieve high short circuit current and open circuit voltage. One of the best candidates for that purpose could be CNTs which have already demonstrated an excellent PV performance when interfaced with Si. Figure 12 shows a hypothetical schematic of a near ideal hybrid solar cells including (i) thin film (mesoporous Si membrane); (ii) 1-D

photonic crystal feature (fabricated by electrochemical etching with alternating layers of high and low porosity); (iii) high interface area between organic and inorganic components due to porous structure; (iv) CNTs inside the straight pores to provide efficient light harvesting, charge separation, transport and collection. However, instead of carbon nanotubes, other organic conductors can also be employed, such as polythiophene derivatives, and discotic liquid crystals, which possess high hole mobilities.

**Figure 12.** Cross sectional view of thin film solar cell based on mesoporous 1-D photonic crystal prepared by electrochemical etching of Si and infiltrated with SWNTs. 1-D photonic crystal is constructed from alternating layers of high and low porosity.



The continuing progress in nanostructuring of Si and other Group IV, III-V semiconductor in conjunction with novel techniques for organic material infiltration and interface optimization promise further advances in the near future to develop a new generation of hybrid PVs.

## References and Notes

1. *Organic Photovoltaics: Materials, Device Physics, and Manufacturing Technologies*; Brabec, C., Scherf, U., Dyakonov, V., Eds.; Wiley-VCH: New York, NY, USA, 2008.
2. Bredas, J.L.; Norton, J.E.; Cornil, J.; Coropceanu, V. Molecular understanding of organic solar cells: The challenges. *Acc. Chem. Res.* **2009**, *42*, 1691–1699.
3. Gunes, S.; Neugebauer, H.; Sariciftci, N.S. Conjugated polymer-based organic solar cells. *Chem. Rev.* **2007**, *107*, 1324–1338.
4. Kim, J.Y.; Lee, K.; Coates, N.E.; Moses, D.; Nguyen, T.Q.; Dante, M.; Heeger, A.J. Efficient tandem polymer solar cells fabricated by all-solution processing. *Science* **2007**, *317*, 222–225.
5. Kim, K.; Liu, J.; Nambhothiry, M.A.G.; Carroll, D.L. Roles of donor and acceptor nanodomains in 6% efficient thermally annealed polymer photovoltaics. *Appl. Phys. Lett.* **2007**, *90*, 163511.
6. Marks, R.N.; Halls, J.J.M.; Bradley, D.D.C.; Friend, R.H.; Holmes, A.B. The photovoltaic response in poly (p-phenylene vinylene) thin-film devices. *J. Phys. Condens. Matter* **1994**, *6*, 1379–1394.
7. Barth, S.; Basler, H. Intrinsic photoconduction in PPV-type conjugated polymers. *Phys. Rev. Lett.* **1997**, *79*, 4445–4448.

8. Grahn, H.T. *Introduction to Semiconductor Physics*; World Scientific Publishing Company: Singapore, 1999.
9. Gratzel, M. Dye-sensitized solar cells. *J. Photochem. Photobiol. C* **2003**, *4*, 145–153.
10. Boucle, J.; Ravirajan, P.; Nelson, J. Hybrid polymer-metal oxide thin films for photovoltaic applications. *J. Mater. Chem.* **2007**, *17*, 3141–3153.
11. Gledhill, S.E.; Scott, B.; Gregg, B.A. Organic and nano-structured composite photovoltaics: An overview. *J. Mater. Res.* **2005**, *20*, 3167–3179.
12. McGehee, M.D. Nanostructured organic-inorganic hybrid solar cells. *Mater. Res. Soc. Bull.* **2009**, *34*, 95–100.
13. Chiba, Y.; Islam, A.; Watanabe, Y.; Komiya, R.; Koide, N.; Han, L. Dye-sensitized solar cells with conversion efficiency of 11.1%. *Jpn. J. Appl. Phys.* **2006**, *45*, L638–L640.
14. Wang, M.; Moon, S.; Xu, M.; Chittibabu, K.; Wang, P.; Cevey-Ha, M.; Humphry-Baker, R.; Zakeeruddin, S.M.; Graetzel, M. Efficient and stable solid-state dye-sensitized solar cells based on a high-molar-extinction-coefficient sensitizer. *Small* **2009**, (in press).
15. Ravirajan, P.; Haque, S.A.; Durrant, J.R.; Poplavskyy, D.; Bradley, D.D.C.; Nelson, J. Hybrid nanocrystalline TiO<sub>2</sub> solar cells with a fluorene–thiophene copolymer as a sensitizer and hole conductor. *J. Appl. Phys.* **2004**, *95*, 1473–1480.
16. Bao, Z.; Dodabalapur, A.; Lovinger, A.J. Soluble and processable regioregular poly(3-hexylthiophene) for thin film field-effect transistor applications with high mobility. *Appl. Phys. Lett.* **1996**, *69*, 4108–4110.
17. Makino, T.; Segawa, Y.; Tsukazaki, A.; Ohtomo, A.; Kawasaki, M. Electron transport in ZnO thin films. *Appl. Phys. Lett.* **2005**, *87*, 022101.
18. Antoniadou, M.; Stathatos, E.; Boukos, N.; Stefopoulos, A.; Kallitsis, J.; Krebs, F.C.; Lianos, P. Study of hybrid solar cells made of multilayer nanocrystalline titania and poly(3-octylthiophene) or poly-(3-(2-methylhex-2-yl)-oxycarbonyldithiophene). *Nanotechnology* **2009**, *20*, 495201.
19. Nelson, J.; Kirkpatrick, J.; Ravirajan, P. Factors limiting the efficiency of molecular photovoltaic devices. *Phys. Rev. B* **2004**, *69*, 035337.
20. Huynh, W.U.; Dittmer, J.J.; Alivisatos, A.P. Hybrid nanorod-polymer solar cells. *Science* **2002**, *295*, 2425–2427.
21. Sailor, M.J.; Ginsburg, E.J.; Gorman, C.B.; Kumar, A.; Grubbs, R.H.; Lewis, N.S. Thin films of n-Si/Poly-(CH<sub>3</sub>)<sub>3</sub>Si-cyclooctatetraene: conducting-polymer solar cells and layered structures. *Science* **1990**, *249*, 1146–1149.
22. Ozaki, M.; Peebles, D.L.; Weinberger, B.R.; Chiang, C.K.; Gau, S.C.; Heeger, A.J.; McDiarmid, A.G. Junction formation with pure and doped polyacetylene. *Appl. Phys. Lett.* **1979**, *35*, 83–85.
23. Govrishankar, V.; Scully, S.R.; McGehee, M.D.; Wang, Q.; Branz, H.M. Exciton splitting and carrier transport across the amorphous-silicon/polymer solar cell interface. *Appl. Phys. Lett.* **2006**, *89*, 252102.
24. Govrishankar, V.; Scully, S.R.; Chan, A.T.; McGehee, M.D.; Wang, Q.; Branz, H.M. Exciton harvesting, charge transfer, and charge-carrier transport in amorphous-silicon nanopillar/polymer hybrid solar cells. *J. Appl. Phys.* **2008**, *103*, 064511.

25. Alet, P.J.; Palacin, S.; Roca, P.; Cabarrocas, I.; Kalache, B.; Firon, M.; de Bettignies, R. Hybrid solar cells based on thin-film silicon and P3HT—A first step towards nano-structured devices. *Eur. Phys. J. Appl. Phys.* **2007**, *36*, 231–234.
26. Matsumoto, Y.; Estrada, M.; Nolasco, J.C. Performance of P3HT/c-Si hybrid solar cell. In Proceedings of the 33rd IEEE Photovoltaic Specialists Conference, San Diego, CA, USA, May 2008.
27. Horowitz, G.; Garnier, F. Polythiophene-GaAs p-n heterojunction solar cells. *Sol. Energy Mater. Sol. Cells* **1986**, *13*, 47–55.
28. Garnier, F. Hybrid organic-on-inorganic photovoltaic devices. *J. Opt. A: Pure Appl. Opt.* **2002**, *4*, S247–S251.
29. Ackermann, J.; Videlot, C.; Kassmi, A.E.; Guglielmetti, R.; Fages, F. Highly efficient hybrid solar cells based on an octithiophene-GaAs heterojunction. *Adv. Funct. Mater.* **2005**, *15*, 810–817.
30. Ackerman, J.; Videlot, C.; Kasami, A.E. Growth of organic semiconductors for hybrid solar cell application. *Thin Solid Films* **2002**, *403*, 157–161.
31. Schmidt-Mende, L.; Fechtenkotter, A.; Mullen, K.; Moons, E.; Friens, R.H.; MacKenzie, J.D. Self-organized discotic liquid crystals for high-efficiency organic photovoltaics. *Science* **2001**, *293*, 1119–1122.
32. Antohe, S.; Tomozeiu, N.; Gogonea, S. Properties of the organic-on-inorganic semiconductor barrier contact diodes in/PTCDI/p-Si and Ag/CuPc/p-Si. *Phys. Status Solidi A* **1991**, *125*, 397–408.
33. Remaki, B.; Guillaud, G.; Mayes, D. Space charge analysis in doped zinc phthalocyanine thin films. *Opt. Mater.* **1998**, *9*, 240–244.
34. El-Nahass, M.M.; Zeyada, H.M.; Aziz, M.S.; El-Ghamaz, N.A. Carrier transport mechanisms and photovoltaic properties of Au/p-ZnPc/p-Si solar cell. *Solid-State Electron.* **2005**, *49*, 1314–1319.
35. Riad, S. Dark and photoelectric conversion properties of p-MgPc/n-Si (organic/inorganic) heterojunction cells. *Thin Solid Films* **2000**, *370*, 253–257.
36. El-Nahass, M.M.; Abd-El-Rahman, K.F.; Farag, A.A.M.; Darwish, A.A. Photovoltaic properties of NiPc/p-Si (organic/inorganic) heterojunctions. *Org. Electron.* **2005**, *6*, 129–136.
37. Karimov, K.; Ahmed, M.M.; Moiz, S.A.; Fedorov, M.I. Temperature-dependent properties of organic-on-inorganic Ag/p-CuPc/n-GaAs/Ag photoelectric cell. *Sol. Energy Mater. Sol. Cells* **2005**, *87*, 61–75.
38. El-Nahass, M.M.; Zeyada, H.M.; Aziz, M.S.; Makhlof, M.M. Current transport mechanisms and photovoltaic properties of tetraphenylporphyrin/n-type silicon heterojunction solar cell. *Thin Solid Films* **2005**, *492*, 290–297.
39. Kuo, C.Y.; Gau, C. Arrangement of band structure for organic-inorganic photovoltaics embedded with silicon nanowire arrays grown on indium tin oxide glass. *Appl. Phys. Lett.* **2009**, *95*, 053302.
40. Liu, C.Y.; Holman, Z.C.; Kortshagten, U.R. Hybrid solar cells from P3HT and silicon nanocrystals. *Nano Lett.* **2009**, *9*, 449–452.
41. Huang, J.S.; Hsiao, C.Y.; Syu, S.J.; Chao, J.J.; Lin, C.F. Well-aligned single-crystalline silicon nanowire hybrid solar cells on glass. *Sol. Energy Mater. Sol. Cells* **2009**, *93*, 621–624.
42. Bi, H.; LaPierre, R.R. A GaAs nanowire/P3HT hybrid photovoltaic device. *Nanotechnology* **2009**, *20*, 465205.

43. Novotny, C.J.; Yu, E.T.; Yu, P.K.L. InP nanowire/polymer hybrid photodiode. *Nano Lett.* **2008**, *8*, 775–779.
44. Du Pasquier, A.; Mastrogiiovanni, D.D.T.; Klein, L.A.; Wang, T.; Garfunkel, E. Photoinduced charge transfer between poly (3-hexylthiophene) and germanium nanowires. *Appl. Phys. Lett.* **2007**, *91*, 183501.
45. Christophersen, M.; Langa, S.; Carstensen, J.; Tiginyanu, I.M.; Foll, H. A comparison of pores in silicon and pores in III-V compound materials. *Phys. Status Solid. A* **2003**, *197*, 197–203.
46. Canham, L.T. *Properties of Porous Silicon*; IEE/Inspec: London, UK, 1997.
47. Levitsky, I.A.; Euler, W.B.; Tokranova, N.; Xu, B.; Castracane, J. Hybrid solar cells based on porous Si and copper phthalocyanine derivatives. *Appl. Phys. Lett.* **2004**, *85*, 6245–6247.
48. Tokranova, N.; Levitsky, I.A.; Xu, B.; Castracane, J.; Euler, W.B. Hybrid solar cells based on organic material embedded into porous silicon. In Proceedings of the SPIE: Organic Photonic Materials and Devices VII, San Jose, CA, USA, January 2005; pp.183–190.
49. Prabakaran, R.; Fortunato, E.; Martins, R.; Ferreira, I. Fabrication and characterization of hybrid solar cells based on copper phthalocyanine/porous silicon. *J. Non-Cryst. Solids* **2008**, *354*, 2892–2896.
50. Komolov, A.S.; Moller, P. Electronic charge distribution at interfaces between Cu-phthalocyanine films and semiconductor surfaces. *Surf. Sci.* **2003**, *532–535*, 1004–1010.
51. Aroutiounian, V.M.; Ghulinyan, M.Z. Electrical conductivity mechanisms in porous silicon. *Phys. Status Solidi A* **2003**, *197*, 462–466.
52. Li, Z.; Kunets, V.P.; Saini, V.; Xu, Y.; Dervishi, E.; Salamo, G.J.; Biris, A.R.; Biris, A.S.  $\text{SOCl}_2$  enhanced photovoltaic conversion of single wall carbon nanotube/n-silicon heterojunctions. *Appl. Phys. Lett.* **2008**, *93*, 243117.
53. Li, Z.; Kunets, V.P.; Saini, V.; Xu, Y.; Dervishi, E.; Salamo, G.J.; Biris, A.R.; Biris, A.S. Light-harvesting using high density p-type single wall carbon nanotube/n-type silicon heterojunctions. *ACS Nano* **2009**, *6*, 1407–1414.
54. Jia, Y.; Wei, J.; Wang, K.; Cao, A.; Shu, Q.; Gui, X.; Zhu, Y.; Zhuang, D.; Zhang, G.; Ma, B.; Wang, L.; Liu, W.; Wang, Z.; Luo, J.; Wu, D. Nanotube–silicon heterojunction solar cells. *Adv. Mater.* **2008**, *20*, 4594–4598.
55. Wei, J.; Jia, Y.; Shu, Q.; Gu, Z.; Wang, K.; Zhuang, D.; Zhang, G.; Wang, Z.; Luo, J.; Cao, A.; Wu, D. Double-walled carbon nanotube solar cells. *Nano Lett.* **2007**, *7*, 2317–2321.
56. Ong, P.L.; Euler, W.B.; Levitsky, I.A. Hybrid solar cells based on single-walled carbon nanotubes/Si heterojunction. *Nanotechnology* **2010**, *21*, 105203.
57. Dresselhaus, M.S.; Dresselhaus, G.; Eklund, P.C. *Science of Fullerenes and Carbon Nanotubes*; Academic Press: San Diego, CA, USA, 1996.
58. Durkop, T.; Getty, S.A.; Cobas, E.; Fuhrer, M.S. Extraordinary mobility in semiconducting carbon nanotubes. *Nano Lett.* **2004**, *4*, 35–39.
59. Xiao, K.; Liu, Y.; Hu, P.; Yu, G.; Wang, X.; Zhu, D. High-mobility thin-film transistors based on aligned carbon nanotubes. *Appl. Phys. Lett.* **2003**, *83*, 150–152.
60. Sankapal, B.R.; Setyowati, K.; Chen, J. Electrical properties of air-stable, iodine-doped carbon-nanotube-polymer composites. *Appl. Phys. Lett.* **2007**, *91*, 173103.

61. Lee, R.S.; Kim, H.J.; Fischer, J.E.; Thess, A.; Smalley, R.E. Conductivity enhancement in single-walled carbon nanotube bundles doped with K and Br. *Nature* **1997**, *388*, 255–257.
62. Chen, J.; Hamon, M.A.; Hu, H.; Chen, Y.; Rao, A.M.; Eklund, P.C.; Haddon, R.C. Solution properties of single-walled carbon nanotubes. *Science* **1998**, *282*, 95–98.
63. Fujiwara, A.; Matsuoka, Y.; Suematsu, H.; Ogawa, N.; Mitano, K.; Katahura, H.; Maniwa, Y.; Suzuki, S.; Achiba, Y. Photoconductivity in semiconducting single-walled carbon nanotubes. *Jpn. J. Appl. Phys.* **2001**, *40*, L1229–L1231.
64. Levitsky, I.A.; Euler, W.B. Photoconductivity of single wall carbon nanotubes under CW NIR illumination. *Appl. Phys. Lett.* **2003**, *83*, 1857–1859.
65. Freitag, M.; Martin, Y.; Misewich, J.A.; Martel, R.; Avouris, P. Photoconductivity of single carbon nanotubes. *Nano Lett.* **2003**, *3*, 1067–1071.
66. Geng, J.; Zeng, T. Influence of single-walled carbon nanotubes induced crystallinity enhancement and morphology change on polymer photovoltaic devices. *J. Am. Chem. Soc.* **2006**, *128*, 16827–16833.
67. Pradhan, B.; Batabyal, S.K.; Pal, A.J. Functionalized carbon nanotubes in donor/acceptor-type photovoltaic devices. *Appl. Phys. Lett.* **2006**, *88*, 093106.
68. Landi, B.J.; Raffaele, R.P.; Castro, S.L.; Bailey, S.G. Single-wall carbon nanotube-polymer solar cells. *Prog. Photovolt. Res. Appl.* **2005**, *13*, 165–172.
69. Ago, H.; Petritsch, K.; Shaffer, M.S.P.; Windle, A.H.; Friend, R.H. Composites of carbon nanotubes and conjugated polymers for photovoltaic devices. *Adv. Mater.* **1999**, *11*, 1281–1285.
70. Bhattacharyya, S.; Kymakis, E.; Amaratunga, G.A. Photovoltaic properties of dye functionalized single-wall carbon nanotube/conjugated polymer devices. *Chem. Mater.* **2004**, *16*, 4819–4823.
71. Kymakis, E.; Koudoumas, E.; Franghiadakis, I.; Amaratunga, G.A. Post-fabrication annealing effects in polymer-nanotube photovoltaic cells. *J. Phys. D: Appl. Phys.* **2006**, *39*, 1058–1062.
72. Rowell, M.W.; Topinka, M.A.; McGehee, M.D.; Prall, H.J.; Dennler, G.; Sariciftci, N.S.; Hu, L.; Gruner, G. Organic solar cells with carbon nanotube network electrodes. *Appl. Phys. Lett.* **2006**, *88*, 233506.
73. Van de Lagemaat, J.; Barnes, T.M.; Rumbles, G.; Shaheen, S.E.; Coutts, T.J.; Weeks, C.; Levitsky, I.; Peltola, J.; Glatkowski, P. Organic solar cells with carbon nanotubes replacing  $\text{In}_2\text{O}_3\text{:Sn}$  as the transparent electrode. *Appl. Phys. Lett.* **2006**, *88*, 233503.
74. Wang, F.; Dukovic, G.; Brus, L.E.; Heintz, T. The optical resonances in carbon nanotubes arise from excitons. *Science* **2005**, *308*, 838–841.
75. Yoon, M.S.; Ahn, K.H.; Cheung, R.W.; Sohn, H.; Link, J.R.; Cunin, F.; Sailor, M.J. Covalent crosslinking of 1-D photonic crystals of microporous Si by hydrosilylation and ring-opening metathesis polymerization. *Chem. Commun.* **2003**, 680–681.